Discontinuous and continuous separation of the monomeric and dimeric forms of human bone morphogenetic protein-2 (BMP-2) from renaturation batches

Ludmila Gueorguieva[1], Luis Felipe Vallejo[2], Ursula Rinas[2], Andreas Seidel-Morgenstern[1,3*]

[1]Otto-von-Guericke-Universität Magdeburg, Institut für Verfahrenstechnik, P.O. Box 4120, D-39106 Magdeburg, Germany

[2]Gesellschaft für Biotechnologische Forschung mbH (GBF), Bereich Bioverfahrenstechnik, Mascheroderweg 1, D-38124 Braunschweig, Germany

[3]Max-Planck-Institut für Dynamik komplexer technischer Systeme, D-39120 Magdeburg, Germany

*Corresponding autor., Tel. +49-391-671-8644; Fax. +49-391-671-2028

E-mail address: anseidel@vst.uni-magdeburg.de

Abstract

Bone morphogenetic protein-2 (BMP-2) is one of the most interesting of the approx. 14 BMPs which belong to the transforming-growth-factor-β (TGF-β) superfamily. BMP-2 induces bone formation and thus plays an important role as a pharmaceutical protein.

Recently *rh*BMP-2 has been produced in form of inactive inclusion bodies in *E. coli*. After solubilization and renaturation the biologically active dimeric form of *rh*BMP-2 can be generated. However, inactive monomers of BMP-2 are also formed during the renaturation process which must be separated from the active dimeric BMP-2. The purpose of this paper is to present a) results of an experimental study of a chromatographic separation of the monomeric and dimeric forms and b) a concept for a continuous countercurrent simulated moving bed (SMB) process. The capacity of heparin as stationary phase was estimated for different salt concentrations in the mobile phase. A simulation study of a three-zone SMB process was performed applying two different salt concentrations in the feed solution and in the desorbent stream.

Keywords

bone morpho-genetic protein-2, gradient elution, continuous countercurrent separation, step gradients

1 Introduction

Bone morphogenetic proteins (BMPs) are multifunctional proteins with a wide range of biological activities [1]. They are involved in the development of many organs and tissues as well as in the establishment of the basic embryonic body plan [2]. BMP-2 is one of the most important of the approximately 14 different BMPs known at present which belong to the transforming–growth-factor-beta (TGF-β) family. It induces bone formation and thus renders it to a protein of pharmaceutical importance [3]. The successful development of BMP-2 containing implants was reported in various cases [4-6]. FDA has approved the first recombinant human BMP-2 containing product aimed for the healing of degenerative disc diseases (Infuse^{TM}, Medtronic, USA).

BMP-2 is a disulfide-bonded dimer. The two subunits are connected by one disulfide bond and have the simple so-called 69-type structure. The monomers have three intrachain disulfide bridges known as cystine knots, which stabilize their structure [7]. The surface of the dimer is very hydrophobic causing the low solubility of BMP-2 in aqueous solutions [7, 8].

Recombinant human BMP-2 can be produced as active protein from mammalian cell cultures [8, 9], or alternatively in form of inclusion bodies from *Escherichia coli* [10, 11].

In the current work BMP-2 has been produced in form of cytoplasmic inclusion bodies [11]. After solubilization of inclusion body proteins, biologically active dimeric BMP-2 is generated by subjecting unfolded and reduced BMP-2 monomers to refolding conditions using an optimised renaturation protocol [12]. The disulfide-bonded dimeric BMP-2 is formed in a slow process concomitant with the gain of the biological activity [13]. During the renaturation process, inactive monomers of BMP-2 are also formed which need to be separated from the active dimeric BMP-2 [11]. A single chromatographic step using heparin as the stationary phase was found to be suitable to obtain highly purified dimeric *rh*BMP-2. To perform the purification a two-step salt gradient was applied. Gradient

processes based on varying the mobile phase strength are widely used in analytical chromatography to improve separations and to reduce cycle times [14-16]. Regarding preparative applications this concept can be realized also in a continuous manner. The implementation of gradients in simulated moving bed (SMB) chromatography was studied theoretically [17-19] and applied experimentally to separate mixtures of proteins [20] and nucleosides [21]. An important supposition for a quantitative understanding of gradient elution is the knowledge of the locally and temporally changing distribution equilibrium during the chromatographic process. For most chromatographic systems these equilibria can be determined only experimentally. Typically, to cover the relevant range of mobile phase compositions the number of experiments is high.

The aim of the present work was to quantify the capacity of the applied heparin stationary phase with respect to the monomeric and dimeric forms of *rh*BMP-2 at different salt concentrations in the mobile phase. For this purpose the relevant adsorption equilibrium constants were estimated for various mobile phase compositions from pulse experiments. Additionally, frontal analysis experiments were carrying out to evaluate the extent of nonlinearity of the isotherms. Based on these data a concept for a continuous three-zone gradient-SMB process for the separation of rhBMP-2 was analysed theoretically. The simulation study performed served to identify suitable operating conditions for such an attractive process.

2 Equilibrium and column models

The quantitative describtion of chromatographic processes requires mainly the knowledge of the underlying thermodynamic equilibria between the mobile phase, the stationary phase and the components in the mixture to be separated [22]. For constant temperature the equilibrium concentrations of a solute in the liquid phase, C_i, and in the stationary

phase, q_i, are related by the adsorption isotherm. In case of diluted solutions linear isotherms hold, i.e.:

$$q_i = K_{H,i} C_i \tag{1}$$

$K_{H,i}$ is the Henry constant of a component i. It is possible to estimate $K_{H,i}$ from experimentally determined retention times, $t_{R,i}$, according to [22]:

$$K_{H,i} = \frac{(t_{R,i} - t_0)\varepsilon}{t_0(1-\varepsilon)} \tag{2}$$

The application of Eq. 2 requires the total porosity ε. The total porosity ε of a chromatographic column can be defined as follows:

$$\varepsilon = \frac{V_l}{V_{col}} \tag{3}$$

where V_{col} represents the volume of the column and V_l the volume of the liquid phase.

Chromatographic processes are often performed exploiting gradients in the mobile phase composition. Such modulations of the eluent strength cause changes of the distribution equilibrium during the separations and have an influence on the Henry constants defined above. In the literature several models have been suggested that describe the relation between the retention factor of an analyte versus the concentration of the modulator [14, 16, 23-27]. Commonly this dependence is nonlinear and often the following simple relationship suggested for adsorption in normal phase systems can be applied [28]:

$$K_{H,i}(C_{salt}) = (p_{1i} C_{salt})^{-p_{2i}} \tag{4}$$

An estimation of the constants p_{1i} and p_{2i} requires a large set of experimental data for the specific chromatographic system considered.

In case of higher concentrations the equilibrium functions connecting the two phases become nonlinear. The dependence between the concentrations C_i and the loadings q_i can be often described by the competitive Langmuir model [22]:

$$q_i = \frac{K_{H,i}(C_{salt})C_i}{1+\sum_{ii=1}^{N} b_{ii}(C_{salt})C_{ii}} \qquad (5)$$

In the above equation N is the number of components. To quantify the effect of the modulator the same relationship as used in Eq. (4) can be assumed empirically also for the constant b_{ii}:

$$b_{ii}(C_{salt}) = (b_{1ii}C_{salt})^{-b_{2ii}} \qquad (6)$$

To describe concentration profiles in chromatographic columns various models are available [22]. A simple tool is provided by the classical cell model introduced by Craig [29]. This model is based on dividing the column into a number, N_c, of cells of equal size. In each of these cells in a first step equilibrium is established between the mobile and stationary phases. In a second step the liquid fraction in a cell is transferred into the next cell in the direction of flow. Feed is injected in the first cell. Each transfer is followed by a new equilibration between the two phases.

The following mass balance equations hold for a cell k, component i and equilibration step j:

$$C_{i,k}^{j+1} - C_{i,k-1}^{j} + \frac{1-\varepsilon}{\varepsilon}(q_{i,k}^{j+1} - q_{i,k}^{j}) = 0 \qquad i = 1,N;\ j = 1,P;\ k = 1,N_c \qquad (7)$$

The time interval for transferring the liquid phase from one cell to the next is $\Delta t = t^{j+1} + t^{j}$. This interval has to be adjusted to the actual flowrate in the column, $\dot{V}$, and is related to the dead time of the column, t_0. Obviously, the following relation has to be fulfilled:

$$\Delta t = \frac{t_0}{N_c} = \frac{\varepsilon V_{col}}{\dot{V}} \qquad (8)$$

Considering an initially ($j=0$) not preloaded column and a rectangular injection profile holds:

$$C_{i,k}^{0} = 0, q_{i,k}^{0} = 0 \ \ for\ all\ k$$

$$C_{i,0}^{j} = \begin{cases} C_{i,inj} & for\ \ j * \Delta t \le t_{inj} \\ 0 & for\ \ j * \Delta t \le t_{inj} \end{cases} \quad i = 1, N;\ k = 1, N_c \tag{9}$$

In Eq.(9) $C_{i,inj}$ is the injection concentration and t_{inj} is the injection time.

3 Experimental

3.1 Chromatographic system and experimental setup

Based on preliminary work [11] the separation of the monomeric and dimeric rhBMP-2 was performed on prepacked HiTrap™ Heparin HP 1 ml columns (Amersham Biosciences, Uppsala, Sweden). This heparin stationary phase is designed for affinity purifications of proteins such as growth factors, coagulation factors, lipoproteins and steroid receptors. The matrix is based on Sepharose HP. A particle size of 34µm was used. The column dimensions were: length L=2.5 cm and diameter d=0.7cm.

As the mobile phase a buffer A (4M urea / 20mM tris-HCl, pH 8.0) was used. The elution buffer contained buffer A and NaCl with concentrations in the range of 0.3 – 0.6M.

To carry out the experiments a BioLogic DuoFlow™ unit (Bio-Rad Laboratories GmbH, München) was applied allowing to perform gradients. UV detection at 280nm was used to quantify the elution profiles. A conductivity monitor allowed the online control of the salt concentration.

3.2 Procedures

Three types of standard chromatographic experiments were performed at ambient temperature using a flowrate of 1.5ml/min in order to estimate a) the porosity and efficiency with the non retained marker, b) the Henry constants for different salt concentrations and c) the isotherm nonlinearities.

a) The porosity, ε, and a number of equilibrium stages, N_c, were measured for seven columns by injecting 0.1% acetone as a non retained tracer, which was detected at the column outlet by measuring UV absorbance at 280nm. Further the plate numbers for the monomer and dimer were estimated from the variances of the peaks.

b) The initial slopes of the adsorption isotherms were determined from pulse experiments with pure monomer or dimer isolated in preliminary runs. For each of the BMP forms 50µl of diluted solutions were injected into a column equilibrated at different salt concentrations (0.18 – 0.60 M NaCl). From the peak widths again the equilibrium stage numbers were estimated for each component.

c) In order to validate the Henry constants obtained from pulse experiments and to estimate possible isotherm nonlinearities, breakthrough curves were recorded under isocratic conditions. As feeds two different batches of previously dialysed and filtrated renaturation mixture [11, 12] were used. The fractions contained contaminants (~ 1% host cell proteins), monomeric and dimeric *rh*BMP-2. The total protein concentration, $C_{BMP\text{-}2}$, was in the range from 0.22 to 0.45 g/l. A variation of the sodium chloride concentrations in the range from 0.10 to 0.22M was performed with a feed solution in which the ratio of monomeric to dimeric *rh*BMP-2 was 3:1. In further experiments devoted to study the effect of the BMP-2 concentration on the course of the breakthrough profile the corresponding ratio was 4:1. For all experiments the initial conductivity of the solutions was observed offline and at the column outlet - online. For each breakthrough curve measured a new column filled with the same stationary phase was used. For the elution of the components a two step salt gradient was performed. Collected fractions were analyzed by SDS-PAGE gel electrophoresis as described before [11, 12]. The experimentally obtained break-through curves were compared with model predictions, in order to validate the Henry-constants and to estimate possible nonlinearities of the adsorption isotherms.

4 Results of the experimental investigations

4.1 Porosity, plate numbers and equilibrium constants

The average porosity of the seven columns characterized was ε=0.89±0.02. For the applied flow rate (1.5 ml/min) the number of equilibrium stages was estimated with acetone as N_c=20. The pulse experiments performed with monomeric and dimeric BMP-2 revealed that the adsorption equilibrium constants depend strongly on the mobile phase composition. In Fig. 1 are shown some of the experimentally determined elution profiles for different salt concentrations. The Henry constants obtained from the pulse experiments using Eq. 2 are summarised in Table 1. Obviously for all salt concentrations the dimeric BMP-2 is the significantly better adsorbed component. Of course the Henry constants for both components decrease with increasing salt concentration. It can be recognized that they differ widely monomeric and dimeric forms when the salt concentration is low. For sodium chloride concentrations lower than 0.45M no elution profile for the dimeric BMP-2 was detected. Therefore the Henry constants given in Table 1 for 0.18M and 0.22M NaCl were estimated from identified breakthrough times in frontal analysis experiments. From the analysis of the breakthrough curves it was further estimated that the contaminants (con) elute with the dead volume of the column, i.e. $K_{H,con}\approx 0$. The obtained equilibrium data were analyzed using Eqs. (1) and (4). The free parameters, resulting from fitting the theoretical to the experimental data, are $p_{1,mon}$=2.4788 [l/g]; $p_{2,mon}$=5.3469 [-]; $p_{1,dim}$=0.6325 [l/g]; $p_{2,dim}$=3.5379 [-]. Fig. 2 illustrates the dependency of the Henry constants on the sodium chloride concentration and the empirical description based on Eq. (4). The analysis of the pulse experiments delivered also estimates for the number of equilibrium stages, N_c, for the monomeric and dimeric *rh*BMP-2. For the range of salt concentrations covered the N_c for the monomer was between 2 and 8. For 0.45M and 0.6M NaCl N_c was found to be appr. 11 for the dimer.

194 **4.2 Breakthrough curves (evaluation of isotherm nonlinearity)**

195 Results of selected breakthrough experiments performed are shown in Figs. 3 and 4.
196 Breakthrough curves were recorded for varied salt (Fig. 3a) and *rh*BMP-2 (Fig.4a) concen-
197 trations. They were analysed in order to evaluate the extent of possible nonlinearities of
198 the adsorption isotherms. The experiments illustrated in Fig. 3a are for the three salt
199 concentrations: 0.10M, 0.18M and 0.22M NaCl. The injected volumes varied between
200 0.45l and 0.56l and were large enough to reach column saturation. The subsequent elution
201 of the bound components was done by applying a two-step salt gradient. In a first step the
202 monomeric *rh*BMP-2 was desorbed with 0.3M NaCl. In a second step the dimeric *rh*BMP-2
203 eluted with 0.6M NaCl. The fractions of these two steps were collected and analysed by
204 SDS-PAGE gel electrophoresis. An example is shown in Fig. 3b. Because of the high
205 purity fraction 2 (dimeric *rh*BMP-2) could be also analysed by UV absorption at 280nm. In
206 Tab. 2 are summarized the concentrations of the feed solutions and characteristic values
207 of the two collected fractions. The injected and collected masses of the dimeric *rh*BMP-2
208 are also presented. Obviously, the highest dimer recovery, REC, was obtained for the salt
209 concentration of 0.22M. In contrast the largest average concentration of collected dimer
210 was found with 0.18M NaCl. Similar results are depicted in Fig. 4a for different *rh*BMP-2
211 concentrations in the feed. In these experiments the used mobile phase contained 0.22M
212 NaCl. An estimation of characteristic retention volumes, $V_{R,i}^{char}$, of the two fronts was done
213 by differentiating the breakthrough curves. The obtained data are shown in Table 3 and
214 Table 4. In order to specify values of $V_{R,mon}^{char}$ for the monomer the second derivative of the
215 signal was used due to difficulties in interpreting the first derivative. The characteristic
216 breakthrough volumes were used for the feed concentration to estimate the isotherm
217 chords. Corresponding values for q_{mon} and q_{dim} are depicted in Fig. 4b. For comparison the
218 values estimated from the experiment with feed 0.22M NaCl and C_{mon}:C_{dim}=3:1 are also
219 specified (open square and open triangle). The estimated data result from analysing the

experiments with two feeds from different renaturation batches. The increased Fig. 3a and Fig. 4a shows that the contaminants differ in both solutions. They affect the behaviour of the monomer. The estimated values of q_{dim} follow the same trend line. The adsorption capacities of the dimer in the range of investigations are not affected from the contaminants and monomer.

With the Henry constants $K_{H,i}$ determined (from the pulse experiments and breakthrough curves) the measured elution profiles were simulated using the Craig-Model (Eq. 7) and the competitive Langmuir isotherm. In two series of calculations the number of the equilibrium stages was set for both mononmeric and dimeric *rh*BMP-2 equally to 11 (as estimated from pulse experiments with the dimer) and 20 (as estimated with acetone). For these simulations the values of the parameter b_{ii} (Eq. 5) were varied between 0 and 1 l/g. The shape of the simulated breakthrough curves differed from the experimental observations essentially because in these simulations the contaminants were not considered. It was found that the number of the equilibrium stages in the range covered had no big influence on the shape of the breakthrough curves. It was further found that a satisfying representation of the shapes of the profiles and of the characteristic retention volumes is achieved for b_{mon}=b_{dim}=0 [l/g] and N_c=20. An increase of the b-values did not lead to significant improvements. A typical result of these simulations is shown in Fig. 5. There are apparently negligible nonlinearity effects in the region of investigations.

5. Theoretical study of continuous separation

5.1 Concept and model

Up to now classical discontinuous elution chromatography has been considered. It is well known that continuous counter-current chromatography concepts based on the simulated moving bed technique might offer distinct advantages e.g. improved productivity, reduced solvent consumption and large product concentrations. The classical SMB process is

based on using a four-zone arrangement [30]. A feature of this process is that there are high requirements on the proper functioning of the corresponding regeneration zone in order to recycle the solvent. For cheap solvents, e.g. aqueous solutions as used often in biotechnology, a regeneration of the solvent might not be needed. Then there are more simple three-zone-configurations available. The corresponding principle of a three-zone true moving bed (TMB) is shown in Fig. 6. To describe four or three-zone TMB processes under steady state conditions again the simple Craig model described above for batch chromatography can be applied after adjusting it to model counter-current chromatography. The main balance equation is [31]:

$$\dot{V}_Z\,(C_{i,k-1}-C_{i,k})+\dot{V}_S\,(q_{i,k+1}(\overline{C}_{i,k+1})-q_{i,k}(\overline{C}_{i,k}))=\dot{V}_{ext}\,C_{ext}$$

$$with \qquad \dot{V}_{ext}\,C_{i,ext}=\begin{cases}-\dot{V}_{Feed}\,C_{i,Feed} & for\ k=F\\ \dot{V}_E\,C_{i,E} & for\ k=E\\ 0 & for\ all\ other\ k\end{cases} \tag{10}$$

$$Z=I,II,III;\quad k=1,N_{c,total}=4+N_c^{I}+N_c^{II}+N_c^{III}$$

$\dot{V}_S$ is the solid-phase flow-rate and the $\dot{V}_Z$ are the liquid-phase flow rates in the zones. For an estimation of three characteristic net flow rates of the mobile and stationary phases the equilibrium theory can be conveniently used assuming an infinite number of cells [32, 33]. The essential operating parameters are the flow-rate ratios in the three zones, m_Z, defined as follows:

$$m_Z=\frac{\dot{V}_Z}{\dot{V}_S}\quad Z=I,II,III \tag{11}$$

In the conventional isocratic process the solvent composition is identical in the whole unit. Then the following inequalities define under linear conditions a region where a diluted binary feed mixture of the two components A and B can be completely resolved [34, 35]:

$$\begin{aligned}&K_{H,B}<m_I\\ &K_{H,A}<m_{II}<m_{III}<K_{H,B}\end{aligned} \tag{12}$$

For realizing a two-step-gradient the solvent strength in the feed stream should be set lower then that in the desorbent stream i.e. $C_{salt}^{Feed} < C_{salt}^{Des}$ (Fig. 6) [e.g. 28, 31]. This leads to different salt concentration in zones *I*, *II* and in zone *III*, and consequently, to the following relation for the Henry constants:

$$K_H^{I,II}(C_{salt}^{I,II} = C_{salt}^{Des}) < K_H^{III}(C_{salt}^{III} = C_{salt}^{III}) \tag{13}$$

Necessary conditions for complete separations for the two-step-gradient TMB mode are then instead of Eq. 12 given by the following inequalities [34]:

$$\begin{aligned} &K_{H,B}^{Des}(C_{salt}^{Des}) < m_I \\ &K_{H,A}^{Des}(C_{salt}^{Des}) < m_{II} < K_{H,B}^{Des}(C_{salt}^{Des}) \\ &K_{H,A}^{R}(C_{salt}^{R}) < m_{III} < K_{H,B}^{R}(C_{salt}^{R}) \end{aligned} \tag{14}$$

Eq. (14) helps to design such three-zone two-step gradient SMB-processes under linear conditions. For specifying concrete operating points for a certain separation problem the flow rates need to be chosen respecting Eq. 14. This can be done by rendering the inequalities into equations by introducing a safety factor β ($\beta > 1$) into the relation for the first zone:

$$m_I = \beta_I K_{H,B}^{Des} \tag{15}$$

This safety factor β_I secures the regeneration of the stationary phase in zone *I*. Suitable operating points for m_{II} and m_{III} located in the middle of the available region can be set as:

$$\begin{aligned} m_{II} &= \frac{K_{H,B}^{Des}(C_{salt}^{Des}) + K_{H,A}^{Des}(C_{salt}^{Des})}{2} \\ m_{III} &= \frac{K_{H,B}^{R}(C_{salt}^{R}) + K_{H,A}^{R}(C_{salt}^{R})}{2} \end{aligned} \tag{16}$$

5.2 Design and simulation study of a three-zone two-step gradient SMB process

After determining the Henry constants K_H characteristic for the described system (monomeric and dimeric *rh*BMP-2) as a function of the salt concentration a systematic simulation

study of a possible three-zone two-step gradient SMB process was performed. This was done using the cell model given with Eq.10. In such cases the separation performance of the process depends solely on the choice of the flow-rate ratios m_Z in the zones of the unit. The used configuration was already illustrated schematically in Fig. 6. The two incoming streams are feed, $\dot{V}_{Feed}$, and desorbent, $\dot{V}_{Des}$. For realizing the two step gradient the salt concentration in the feed stream has to be set lower than that in the desorbent stream. Calculations were made at first as a reference under isocratic conditions using $C_{salt}^{Feed} = C_{salt}^{Des} = 0.18\ M$ (point a) and then for four variants of the gradient mode (points b, c, d, e) using two different salt concentrations in the feed (0.18M and 0.20M NaCl) and in the desorbent (0.40M and 0.30M). The values of C_{salt}^{Feed} and C_{salt}^{Des} used are summarised in Table 5 together with the results of the simulations. The considered 1:1 feed mixture had the following concentrations $C_{mon}^{Feed} = C_{dim}^{Feed} = 0.25\ g/l$. The feed flow rate $\dot{V}_{Feed}$ was set as *1 ml/min* which is a realistic value for the column size used in this study. The calculations were done for column with cell number of 20 per zone. The safety factor for zone *I* was $\beta_I = 1.5$. For the selected salt concentrations the isotherm parameters depends strongly on the mobile phase composition (see Fig. 2).The results of the theoretical study are presented in Fig. 7. At first the determined separation regions for the isocratic and variants of the two-step gradient process are shown in the m_{II} – m_{III} – plane in Fig. 7 (left). The operating conditions considered are in the point of gravity of the triangle (a) and in the middle of the region according to Eq. 16 (b-e). The separation region estimated for the isocratic case is larger than for the gradient cases. In Table 5 are summarized the resulting values for the desorbent flow rate, $\dot{V}_{Des}$, the salt concentration in zone *III*, C_{salt}^{III}, the Henry constants, $K_{H,i}^{Z}$, and the flow rate ratios in the three zones, m_K. In the right part of Fig. 7 are shown the theoretical internal concentration profiles for the selected operating conditions. The predicted positions for feed and extract and the concentrations of the

components in the feed mixture are marked. The theoretical concentrations of the dimer at the extraction port, $C_{dim}^{E,theor}$, are given in Tab.5. For the monomer in all cases holds $C_{mon}^{E,theor} = 0$ g/l, i.e. the dimer purity at the extract port is 100%. The theoretical concentration of the dimer in the waste (raffinate) stream is always zero. This stream contains monomeric rhBMP-2 and contaminants and might be collected and used for further renaturations. The accomplished study shows that for points (a) (isocratic conditions) and (b) (gradient C_{salt}^{Feed}=0.20M, C_{salt}^{Des}=0.30M) there is a significant dilution at the extract port in comparison with the feed concentration. In contrast the maximum product (dimer) concentration is found for the selected operating conditions of point (e). The enrichment factor is app. 5. Thus, it can be generalised that the application of the described three-zone two-step gradient SMB process possesses the potential to increases the dimer concentration at the extract port significantly.

6. Conclusions

The separation of the dimeric *rh*BMP-2 from its monomeric form was studied experimentally using batch chromatography in a single column. At first the adsorption equilibrium constants were estimated at different salt concentrations from pulse experiments. Frontal analysis experiments for different initial component and salt concentrations were performed and characteristic breakthrough times and plateau concentrations were identified. Possible nonlinearities of the adsorption isotherms were found to be negligible in the range of investigations. The results of the performed simulations using the Craig cell model revealed a good agreement with experimental profiles for the single column experiments. In a second part a rather simple concept for a new three-zone continuous counter-current process was suggested. Main innovative focus was to implement a two-step salt gradient. The simulation study revealed possible process parameters and conditions for efficient separation using this concept. Of particular interest is the possible enrichment of the desired BMP-2 dimer in the extract stream of such a

process. Further work is currently be focused on the experimental realization of the new process suggested.

Acknowledgements

The financial support of Deutsche Forschungsgemeinschaft / Sonderforschungsbereich (SFB) 578 is gratefully acknowledged.

References

[1] M. Kawabata, T. Imamura, K. Miyazono, Signal Transduction by Bone morphogenetic proteins. Cytokine&Growth Factor Rev. 9 (1998), 1, 49-61

[2] B.L.M. Hogan, Bone morphogenetic proteins: multifunctional regulators of vertebrate development. Genes Dev. 10 (1996), 1580-1594.

[3] R.H. Li, J.M. Wozney, Delivering on the promise of bone morphogenetic proteins. Trends Biotechnol. 19 (2001), 255-265

[4] S.D. Boden, Th.A. Zdeblick, H.S. Sandhu, The use of rhBMP-2 in inter-body fusion cages, Spine 25 (2000), 3, 376-381.

[5] A. Valentin-Opran, J. Wozney, C. Csimma, L. Lilly, G.E. Riedel, Clinical evaluation of recombinant human bone morphogenetic protein-2. Clin. Orthop. 395 (2002), 110-120.

[6] H.S. Sandhu, Bone Morphogenetic proteins and spinal surgery. Spine 28 (2003), 155, 64-73.

[7] C. Scheufler, W. Sebald, M. Hülsmeyer, Crystal structure of human bone morphogenetic protein-2 at 2,7 Å resolution. J. Mol. Biol. 287 (1999), 103-115.

[8] E.A. Wang, V. Rosen, J.S. D'Alessandro, M. Bauduy, P. Cordes, T. Harada, D.I. Israel, R.M. Hewick, K.M. Kerns, P. LaPan, D.P. Luxemburg, D. McQuaid, I.K. Moutsatsos, J. Nove, J.M. Wozney, Recombinant human bone morphogenetic protein induces bone formation. Proc. Natl. Acad. Sci. USA 87 (1990), 2220-2224.

[9] D.I. Israel, J. Nove, K.M. Kerns, I.K. Moutsatsos, R.J. Kaufman, Expression and characterization of bone morphogenetic protein-2 in chinese hamster ovary cells. Growth Factors 7 (1992), 139-150.

[10] R. Ruppert, E. Hoffmann, W. Sebald, Human bone morphogenetic protein 2 contains a heparin-binding site which modifies its biological activity. Eur. J. Biochem. 237 (1996), 295-302.

[11] L.F. Vallejo, M. Brokelmann, S. Marten, S., Trappe, J. Cabrera-Crespo, A. Hoffmann, G. Gross, H. Weich, U. Rinas, Renaturation and purification of bone morphogenetic protein-2 produced as inclusion bodies in high-cell-density cultures of recombinant Escherichia coli. J. Biotechnology 94 (2002), 185-194.

[12] L.F. Vallejo, U. Rinas, Optimized procedure for renaturation of recombinant human bone morphogenetic protein-2 at high protein concentration. Biotechnol. Bioeng. 85 (2004), 601-609.

[13] J. Wendler, L.F. Vallejo, U. Rinas, U. Bilitewski, Application of an SPR-based receptor assay for the determination of biologically active recombinant bone morphogenetic protein-2. Anal. Bioanal. Chem. 381 (2005), 1056-1064.

[14] L.R. Snyder, Principles of adsorption chromatography, Marcel Dekker, New York, 1968.

[15] L.R. Snyder, M.A. Stadalius, in C. Horvath (Editor), High performance liquid chromatography – advances and perspectives, Vol. 4, Academic Press, New York, 1986, p. 208-316.

[16] P. Jandera, J. Churacek. Gradient elution in column liquid chromatography. Elsevier, Amsterdam, 1985

[17] T.B. Jensen, T.G.P. Reijns, H.A.H. Billiet, L.A.M. van der Wielen, Novel simulated moving bed method for reduced solvent consumption. J. Chromatogr. A 873 (2000), 149.

[18] D. Antos, A. Seidel-Morgenstern, Application of gradients in the simulated moving bed process. Chem. Eng. Sci. 56 (2001), 6667-6682.

[19] S. Abel, M. Mazzotti, M. Morbidelli, Solvent gradient operation of simulated moving beds: I. Linear isotherms, J.Chromatogr. A 944 (2002), 23-39.

[20] J. Houwing, S.H. Van Hateren, H.A.H. Billiet, L.A.M. van der Wielen, Effect of salt gradients on the separation of dilute mixtures of proteins by ion-exchange in simulated moving beds. J.Chromatogr.A 952 (2002), 85-98.

[21] S. Abel, M.U. Bäbler, C. Arpagaus, M. Mazzotti, J. Stadler, Two-fraction and three-fraction continuous simulated moving bed separation of nucleosides, J.Chromatogr. A 1043 (2004), 201-210.

[22] G. Guiochon, S. Golshan-Shirazi, A.M. Katti, Fundamentals of preparative and nonlinear chromatography, Boston, MA: Academic Press, 1994.

[23] L.R. Snyder, J.W. Dolan, P.W. Carr, The hydrophobic-substraction model of reversed-phase column selectivity. J.Chromatogr. A 1060 (2004), 77-116.

[24] E. Soczewinski, Solvent composition effects in thin-layer chromatography systems of the type of silica gel-electron donor solvent. Analytical Chemistry 41 (1969), 179-182.

[25] P. Jandera, Gradient elution in normal-phase high-performance liquid chromatographic systems. J.Chromatogr. A 965 (2002), 239-261.

[26] F.D. Antia, C. Horvath, Gradient elution in non-linear preparative liquid chromatography. J.Chromatogr. A 484 (1989), 1-27.

[27] A. Seidel-Morgenstern, Preparative gradient chromatography. Chem. Eng. Technol. 28 (2005), 11, 1265-1273.

[28] D. Antos, A. Seidel-Morgenstern, Two-step solvent gradients in simulated moving bed chromatography, J.Chromatogr. A 944 (2002), 77-91.

[29] L.C. Craig, J. Biological Chemistry 155 (1944), 519-524.

[30] C.B. Broughton, C.G. Gerhold, US Patent 2 985 589, 1961.

[31] D. Beltscheva, P. Hugo, A. Seidel-Morgenstern, Linear two-step gradient counter-current chromatography Analysis based on a recursive solution of an equilibrium stage model, J.Chromatogr. A 989 (2003), 31-45.

[32] M. Mazzotti, G. Storti, M. Morbidelli, Robust design of countercurrent adsorption separation processes: 2. Multicomponent systems. AIChE J. 40 (1994), 1825.

[33] M. Mazzotti, G. Storti, M. Morbidelli, Robust design of countercurrent adsorption separation processes: 3. Nonstoichiometric systems. AIChE J. 42 (1996), 2784.

[34] M. Mazzotti, G. Storti, M. Morbidelli, Optimal operation of simulated moving bed units for nonlinear chromatographic separations. J.Chromatogr.A 769 (1997), 3.

[35] M. Mazzotti, G. Storti, M. Morbidelli, Robust design of countercurrent adsorption separation processes: 5. Nonconstant selectivity. AIChE J. 46 (2000), 1384.

Captions for Tables

1. Henry constants, K_H, experimentally determined from pulse and frontal analysis (*) experiments.
2. Properties of the feed and of the collected fractions. Influence of the salt concentration on the breakthrough and elution behaviour.
3. Experimentally determined characteristic breakthrough times $V_{R,i}^{char}$ for the monomeric and dimeric rhBMP-2 as a function of the salt concentration.
4. Experimentally determined characteristic breakthrough times $V_{R,i}^{char}$ for the monomeric and dimeric rhBMP-2 as a function of the feed concentrations.
5. Parameters used for the simulation study represented in Fig. 7. $C_{mon}^{Feed} = C_{dim}^{Feed} = 0.25 g/l$, $\dot{V}_{Feed} = 1 ml/min$

Table 1:

Henry constants, K_H, experimentally determined from pulse and frontal analysis (*) experiments.

	Henry constants		
C_{salt} [M]	$K_{H,con}$ [-]	$K_{H,mon}$ [-]	$K_{H,dim}$ [-]
0.18	≈ 0	75.52	2167*
0.22		22.20	1108*
0.30		11.08	-
0.40		3.38	-
0.45			0.432
0.60			0.061

Table 2:

Properties of the feed and of the collected fractions. Influence of the salt concentration on the breakthrough and elution behaviour.

C_{salt}	Feed		Fraction 1*		Fraction 2*			$m_{dim}^{capacity}$**	$m_{dim}^{recovered}$***	$Rec = \frac{m_{dim}^{recovered}}{m_{dim}^{injected}}$
	C_{mon}^{Feed}	C_{mon}^{Feed}	V_1 [Interval]	$\overline{C}_{dim,1}^{SDS}$	V_2 [Interval]	$\overline{C}_{dim,2}^{SDS}$	$\overline{C}_{dim,2}^{UV\,280}$			
[M]	[g/l]	[g/l]	[l]	[g/l]	[l]	[g/l]	[g/l]	[g]	[g]	[-]
0.22	0.224	0.071	0.0105 [0,578-0,5885]	0.018	0.006 [0,595-0,601]	0.871	0.881	0.0068	0.0055	0.81
0.18	0.248	0.087	0.0105 [0,511-0,5215]	0.107	0.012 [0,527-0,539]	1.000	1.031	0.0237	0.0135	0.57
0.10	0.262	0.091	0.0105 [0,4695-0,480]	0.083	0.011 [0,485-0,496]	0.921	0.940	-	0.0113	-

* Collected manually based on course of detector signal

** $m_{dim}^{capacity} = c_{dim}^{Feed} V_{R,dim}^{char}$

** $m_{dim}^{recovered} = V_1 \overline{C}_{dim,1}^{SDS} + V_2 \overline{C}_{dim,2}^{UV\,280}$

Table 3:

Experimentally determined characteristic breakthrough times $V_{R,i}^{char}$ for the monomeric and dimeric rhBMP-2 as a function of the salt concentration.

C_{salt} * [M]	$V_{R,i}^{char}$ [ml]	
	Monomer	Dimer
0.10	19.53	-
0.18	6.14	272.9
0.22	2.36	95.8

* C_{mon}^{Feed}, C_{dim}^{Feed} (Table 2)

Table 4:

Experimentally determined characteristic breakthrough times $V_{R,i}^{char}$ for the monomeric and dimeric rhBMP-2 as a function of the feed concentrations.

C_{mon}	C_{dim}	$C_{BMP\text{-}2}$	$V_{R,i}^{char}$ [ml]	
[g/l]	[g/l]	[g/l]	Monomer	Dimer
0,355	0,093	0.45	2.18	44.1
0,226	0,054	0.28	2.52	82.7
0,174	0,044	0.22	2.91	131.4

Table 5:

Parameters used for the simulation study represented in Fig. 7. $C_{mon}^{Feed} = C_{dim}^{Feed} = 0.25 g/l$, $\dot{V}_{Feed} = 1 ml/min$.

	a	b	c	d	e
C_{salt}^{Feed} [M]	0.18	0.20	0.18	0.20	0.18
C_{salt}^{Des} [M]	0.18	0.30		0.40	
C_{salt}^{III} [M]	0.18	0.26	0.219	0.226	0.198
$\dot{V}_{Des}$ [ml/min]	3.41	4.5	1.43	0.45	0.263
$K_{H,mon}^{I,II}$ [-]	74.80	4.872		1.046	
$K_{H,dim}^{I,II}$ [-]	2180	357.9		129.3	
$K_{H,mon}^{III}$ [-]	74.80	10.40	26.15	22.01	45.1
$K_{H,dim}^{III}$ [-]	2180	591.1	1088	970.1	1560
m_I [-]	2399	536.8		194.0	
m_{II} [-]	776.4	181.4		65.19	
m_{III} [-]	1480	300.7	556.8	496.3	802.9
$C_{dim}^{E,theor}$ [g/l]	0.09	0.08	0.26	0.83	1.42

Captions for Figures

1. Influence of the salt concentration on the elution of the monomeric and dimeric *rh*BMP-2. a) monomer: $C_{salt}=0.4\ M$ ($C_{mon}=0.052\ g/l$, solid); $C_{salt}=0.3\ M$ ($C_{mon}=1.10\ g/l$, dashed); $C_{salt}=0.22\ M$ ($C_{mon}=0.85\ g/l$ (dotted); $C_{salt}=0.18\ M$ ($C_{mon}=0.73\ g/l$, solid). b) dimer: $C_{salt}=0.6\ M$ ($C_{dim}=0.074\ g/l$, solid); $C_{salt}=0.45\ M$ ($C_{mon}=0.041\ g/l$, dashed). Parameters: injected volume $V_{inj}= 50\ \mu l$, flow rate $\dot{V}=1.5\ ml/min$.

2. Henry constants $K_{H,i}$ for the monomeric (squares) and dimeric (triangles) rhBMP-2 obtained from pulse experiments and breakthrough curves as a function of the salt concentration. The solid lines represents the dependence specified by Eq. (4) with $p_{1,mon}=2.4788$ [l/g]; $p_{2,mon}=5.3469$ [-]; $p_{1,dim}=0.6325$ [l/g]; $p_{2,dim}=3.5379$ [-].

3. a) Influence of the salt concentration on the breakthrough and elution behaviour for: $C_{salt}=0.22\ M$ (solid), $C_{salt}=0.18\ M$ (dashed), $C_{salt}=0.10\ M$ (dotted). b) SDS-PAGE analysis of feed solutions and fractions 1 and 2 (see text). Lane 1, protein standard; Lanes 2, 5 and 8 represent the feed solutions. Lanes 2 to 4 $C_{salt}=0.10\ M$. Lanes 5 to 7 $C_{salt}=0.18\ M$. Lanes 8 to 10 $C_{salt}=0.22\ M$. Lanes 3, 6 and 9 correspond to fractions 1; lanes 4, 7 and 10 correspond to fractions 2. The small and the big arrows point to monomeric and dimeric *rh*BMP-2, respectively.

4. a) Experimentally determined breakthrough curves for different feed concentrations of the components: $C_{mon}: C_{dim}=4:1$; $C_{BMP\text{-}2}= 0.45\ g/l$ (solid); $C_{BMP\text{-}2}= 0.28\ g/l$ (dashed); $C_{BMP\text{-}2}= 0.22\ g/l$ (dotted). In all case: $C_{salt}=0.22\ M$. b) Estimated equlibrium values for q_{dim} (top, closed triangles) and q_{mon} (bottom, closed squares). Open triangle and open square – values for q_{dim} and q_{mon} estimated from experiment with feed C_{mon}:C_{dim}=3:1 and 0.22M NaCl.

5. Experimental and predicted breakthrough behaviour using the Craig model Eq. (7) and the competitive Langmuir isotherm Eq. (5). Parameters: $C_{salt}=0.22\ M$, $C_{mon}=0.226\ g/;\ C_{dim}=0{,}054\ g/l$; $b_{mon}=0\ l/g$ (solid),; $V_{R,i}^{char}$ as in Table 4. Experimental: top. Simulated: bottom for $N_c=20$, $b_{dim}=0\ l/g$ (solid); $N_c=11$, $b_{dim}=0\ l/g$ (dashed); $N_c=11$, $b_{dim}=0.2\ l/g$ (dotted) .

6. Schematic representation of the principle of a TMB process with the following features: three-zone (open loop) two-step salt gradient. A=dimeric *rh*BMP-2, B=monomeric *rh*BMP-2, C= contaminants

7. Simulation study of possible separation of the monomeric and dimeric *rh*BMP-2 for different operating conditions. Left: separation regions in the m_{II}-m_{III} plane. Right: simulated internal concentration profiles for the isocratic (a) and gradient mode (b, c, d, e). The dashed and dotted lines indicate the concentration profiles of dimeric and monomeric *rh*BMP-2, respectively. The thin solid lines mark the (identical) feed concentration. The arrows indicate the feed (F) and extract (E) ports.

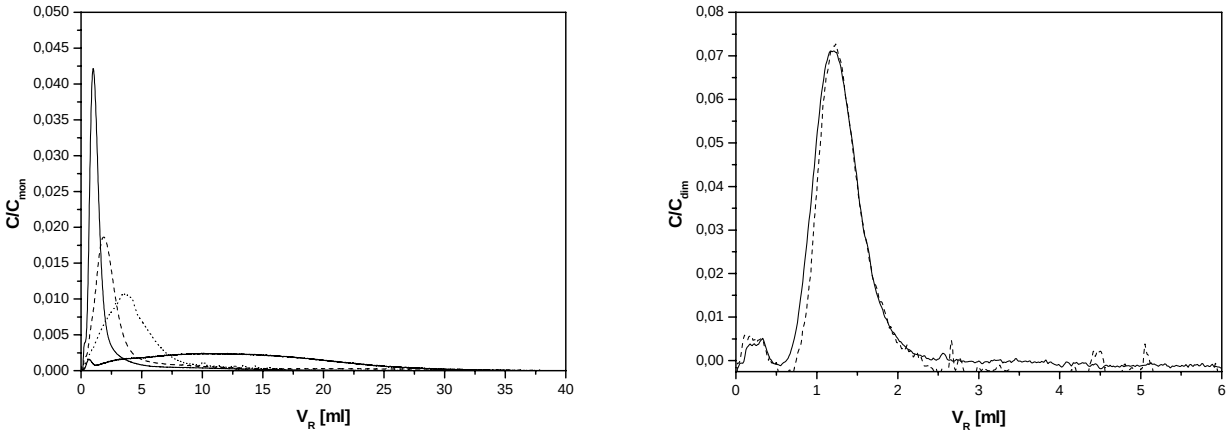

a) b)

Figure 1:

Influence of the salt concentration on the elution of the monomeric and dimeric rhBMP-2. a) monomer*:* C_{salt}*=0.4 M* (C_{mon}*=0.052 g/l*, solid); C_{salt}*=0.3 M* (C_{mon}*=1.10 g/l*, dashed); C_{salt}*=0.22 M* (C_{mon}*=0.85 g/l* (dotted); C_{salt}*=0.18 M* (C_{mon}*=0.73 g/l*, solid). b) dimer: C_{salt}*=0.6 M* (C_{dim}*=0.074 g/l*, solid); C_{salt}*=0.45 M* (C_{mon}*=0.041 g/l*, dashed). Parameters: injected volume V_{inj}*= 50 µl*, flow rate $\dot{V}$ *=1.5 ml/min*.

534

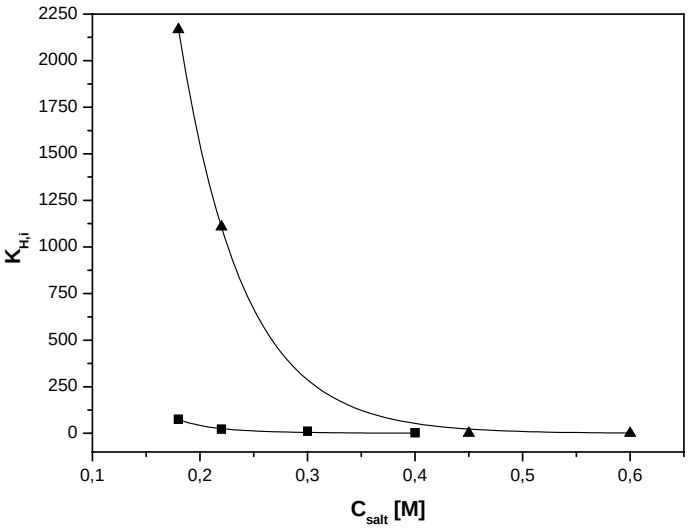

Figure 2:

535

536 Henry constants $K_{H,i}$ for the monomeric (squares) and dimeric (triangles) rhBMP-2
537 obtained from pulse experiments and breakthrough curves as a function of the salt
538 concentration. The solid lines represents the dependence specified by Eq. (4) with
539 $p_{1,mon}=2.4788$ [l/g]; $p_{2,mon}=5.3469$ [-]; $p_{1,dim}=0.6325$ [l/g]; $p_{2,dim}=3.5379$ [-].

540

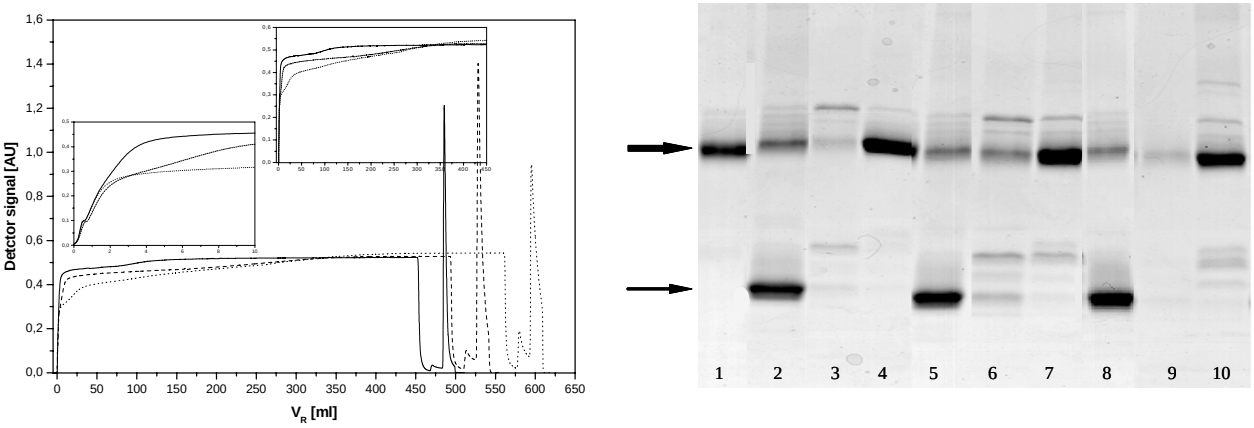

a) b)

Figure 3:

a) Influence of the salt concentration on the breakthrough and elution behaviour for: C_{salt}=*0.22 M* (solid), C_{salt}=*0.18 M* (dashed), C_{salt}=*0.10 M* (dotted). b) SDS-PAGE analysis of feed solutions and fractions 1 and 2 (see text). Lane 1, protein standard; Lanes 2, 5 and 8 represent the feed solutions. Lanes 2 to 4 C_{salt}=*0.10 M*. Lanes 5 to 7 C_{salt}=*0.18 M*. Lanes 8 to 10 C_{salt}=*0.22 M*. Lanes 3, 6 and 9 correspond to fractions 1; lanes 4, 7 and 10 correspond to fractions 2. The small and the big arrows point to monomeric and dimeric *rh*BMP-2, respectively.

554

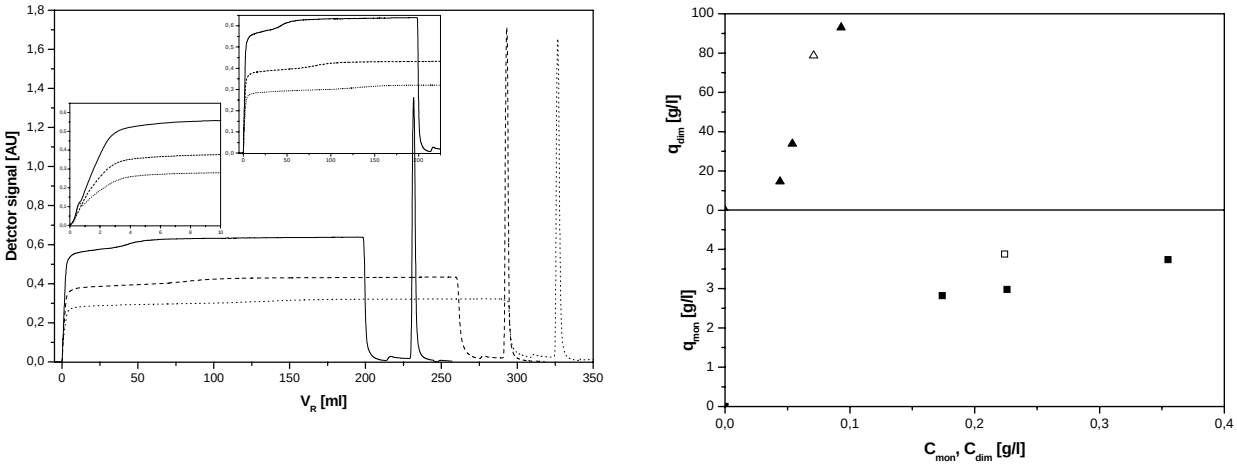

a) b)

Figure 4:

555

556

557 a) Experimentally determined breakthrough curves for different feed concentrations of
558 the components: C_{mon}: C_{dim} =4:1; $C_{BMP\text{-}2}$= 0.45 g/l (solid); $C_{BMP\text{-}2}$= 0.28 g/l (dashed); $C_{BMP\text{-}2}$= 0.22 g/l (dotted). In all case: C_{salt}=0.22 M. b) Estimated equlibrium values for q_{dim} (top,
560 closed triangles) and q_{mon} (bottom, closed squares). Open triangle and open square –
561 values for q_{dim} and q_{mon} estimated from experiment with feed 0.22M NaCl and
562 C_{mon}:C_{dim}=3:1.

563

564

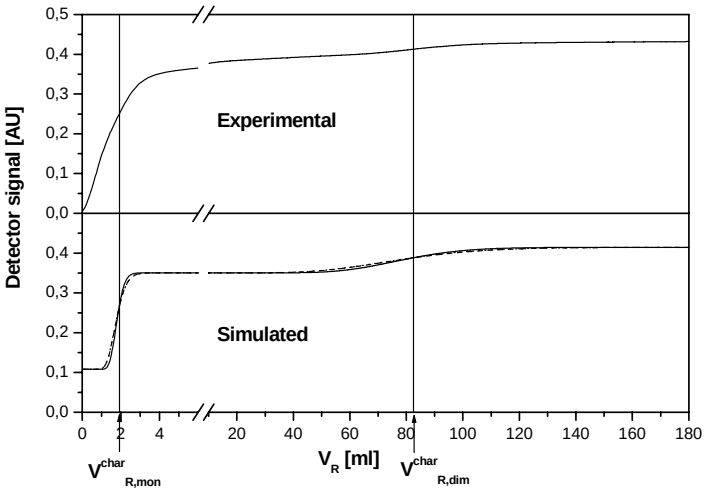

Figure 5:

565

566 Experimental and predicted breakthrough behaviour using the Craig model Eq. (7) and
567 the competitive Langmuir isotherm Eq. (5). Parameters: C_{salt}=0.22 *M*, C_{mon}=0.226 *g/;* C_{dim}
568 =0,054 *g/l*; b_{mon}=0 *l/g* (solid),; $V_{R,i}^{char}$ as in Table 4. Experimental: top. Simulated: bottom
569 for N_c=20, b_{dim}= 0 *l/g* (solid); N_c=11, b_{dim}= 0 *l/g* (dashed); N_c=11, b_{dim}= 0.2 *l/g* (dotted) .

570

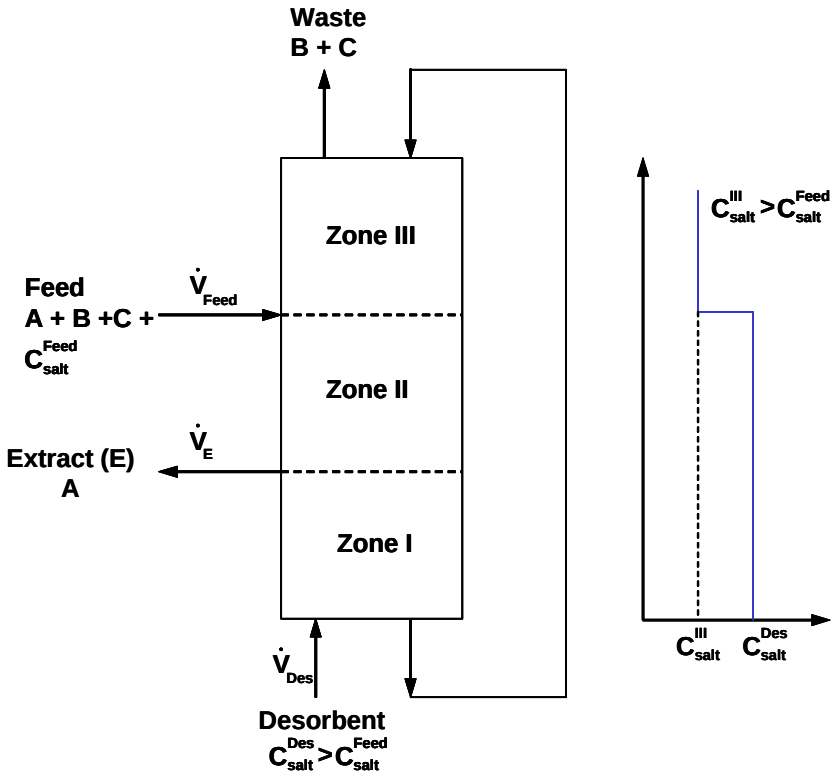

Figure 6:

571

572

573 Schematic representation of the principle of a TMB process with the following futures:
574 open loop, three zone, two-step salt gradient. A=dimeric *rh*BMP-2, B=monomeric
575 *rh*BMP-2, C= contaminants

576

577

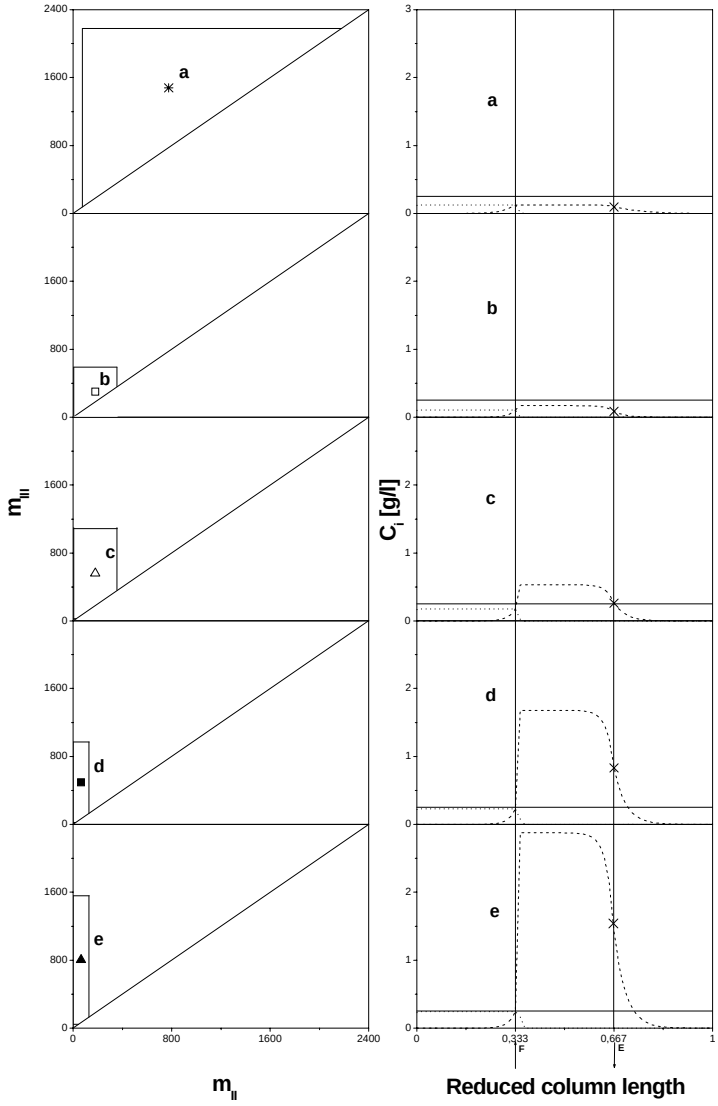

Figure 7:

Simulation study of possible separation of the monomeric and dimeric *rh*BMP-2 for different operating conditions. Left: separation regions in the m_{II}-m_{III} plane. Right: simulated internal concentration profiles for the isocratic (a) and gradient mode (b, c, d, e). The dashed and dotted lines indicate the concentration profiles of dimeric and monomeric *rh*BMP-2, respectively. The thin solid lines mark the (identical) feed concentration. The arrows indicate the feed (F) and extract (E) ports. The crosses mark the product (dimer) concentrations, $C_{dim}^{E,theor}$ (Table 5).